HHS Public Access

Author manuscript

*Macromol Rapid Commun*. Author manuscript; available in PMC 2022 October 01.

Published in final edited form as:

*Macromol Rapid Commun*. 2021 October ; 42(20): e2100372. doi:10.1002/marc.202100372.

# Emergence of Non-Hexagonal Crystal Packing of Deswollen and Deformed Ultra-Soft Microgels Under Osmotic Pressure Control

**Dr. Molla R. Islam**,
Schmid College of Science and Technology, Chapman University, Orange, CA 92780 USA

**Rachel Nguyen**,
Schmid College of Science and Technology, Chapman University, Orange, CA 92780 USA

**Prof. L. Andrew Lyon**
Dale E. and Sarah Ann Fowler School of Engineering, Chapman University, Orange, CA 92866 USA

## Abstract

Highly solvent swollen poly(N-isopropylacrylamide-co-acrylic acid) microgels were synthesized without exogenous crosslinker, making them extremely soft and deformable. These ultralow crosslinked microgels (ULC) were incubated under controlled osmotic pressure to provide a slow (and presumably thermodynamically controlled) approach to higher packing densities. We find that ULC microgels show stable colloidal packing over a very wide range of osmotic pressures and thus packing densities. We also make the surprising observation of co-existence between hexagonal and square lattices over the lower range of studied osmotic pressures, with microgels apparently changing shape from spheres to cubes in defects or grain boundaries. We propose that the unusual packing behavior observed for ULC microgels is due to the extreme softness of these particles, where deswelling causes deformation and shrinking of the particles that result in unique packing states governed by contributions to the entropy at the colloidal system, single particle and ionic levels. These observations further suggest that more detailed experimental and theoretical studies of ultra-soft microgels are required to obtain a complete understanding of their behavior in packed and confined geometries.

## Graphical Abstract


lyon@chapman.edu .

Conflicts of interest

Dr. Lyon is a co-founder and holder of an equity stake in SelSym Biotech, Inc., an early-stage biotechnology company aimed at commercializing artificial platelet technologies based on ULC microgels.

Highly solvent-swollen, ultralow crosslinked microgels (ULCs) show stable colloidal packing over a wide range of applied osmotic pressures. Surprisingly, observed packing structures include the coexistence of hexagonal and square lattices over a narrow range of applied pressures, with the particle shape shifting from spherical (hexagonal lattices) to cubic (square lattices) in a dynamic fashion during interconversion from one symmetry to the other. This observation suggests significant complexity in the physics of ultra-soft microgels in confinement, which warrants deeper computational and experimental investigation of the packing of ultra-soft colloidal particles.

**Keywords**

ultra-soft microgels; osmotic pressure; particle deformation; non-hexagonal packing; cubic lattice

## 1. Introduction

Microgels are colloidal particles composed of a crosslinked polymer network where the particle softness can be tuned by controlling the amount of crosslinker, changing the reaction conditions, and/or by choice of monomers.[1] For the most part, the softness of microgel particles originates from the flexibility of the polymer chains and the length of the chains between crosslinks. Their network structure makes microgels highly porous and deformable, and their softness largely dominates their characteristics in solution, which can deviate strongly from the characteristics of hard spheres.[2]

One of the less common poly(*N*-ispopropylacrylamide) (pNIPAm) microgel types is the ultra-low crosslinked (ULC) microgel, which is synthesized without addition of exogenous crosslinker. ULC microgels show unique swelling and deformation properties compared to crosslinked microgels of similar chemical composition and size.[3] Their network stability/connectivity comes from rare chain branching phenomena, which produce the crosslinking/branch points in the microgel network,[3c] with the effective crosslinking densities in those soft particles estimated to be less than 0.1%. Whereas the utility of these unique structures is still an area of active investigation, we and others have demonstrated that the extreme softness of ULC microgels makes them ideal for advanced biomedical applications, such as in the development of artificial platelets.[4] To support the further development of such applications, we have recently studied temperature and pH induced morphological changes of ULC particles in detail.[5]

The controllable softness of microgels is the most fundamental and perhaps least well understood characteristics that makes them suitable for a diverse range of applications.[3b, 4a, 6] In particular, tuning the softness of microgels and predicting how their mechanical properties control their behavior in crowded environments such as biological systems is essential. Soft particles can respond to a crowded environment by shrinking, deforming, or interpenetrating, which are all controlled by the particle softness and chain topology, and whereas we understand the packing of hard spheres and semi-soft colloids relatively well,[7] we are still unable to predict the complexity of packing of extraordinarily soft and deformable particles such as ULC microgels.

In this paper, we explored the packing of negatively charged poly(N-isopropylacrylamide-co-acrylic acid) ULC microgels, using a slow and presumably gentle method of particle concentration. To control ULC microgel packing densities, the microgels were dialyzed against poly (ethylene glycol) (PEG) solutions of various concentrations to exert different osmotic pressures, and the microgel packing state was analyzed using brightfield microscopy. We find that ULC microgels can pack over a wide range of concentrations and that they crystallize in a random hexagonal closed packed (hcp) lattice in a similar fashion to hard spheres and crosslinked microgels. However, we also observe ULC microgel packing into square lattices that are in co-existence with hcp crystals. Furthermore, the individual microgels packed in square lattices appear to adopt a cubic shape, which then relaxes to a spherical shape at crystal defect sites, or upon conversion into hcp crystals. We propose that this unusual behavior arises from the extreme mechanical softness of ULC microgels, which can accommodate deswelling and deformation to balance the ionic, macromolecular, and colloidal contributions to the overall entropy of the system.

## 2. Results and Discussion

In this study, we used thermoresponsive pNIPAmAAc5 microgels, which are negatively charged at pH values above ~4 due to the presence of comonomer acrylic acid. In the absence of a charged comonomer, ULC microgels are known to have a very low charge density compared to their crosslinked counterparts.[8] Our previous studies revealed that negatively charged pNIPAMAAc5 ULC microgels are highly deformable, as evidenced by their ability to translocate through pores smaller than their hydrodynamic diameter under relatively modest pressure differentials (~70 mmHg).[3c, 9] However, like traditional crosslinked pNIPAm-AAc microgels, they still undergo pH and temperature-induced swelling/deswelling transitions that are predictable based on the identities and ratios of the different co-monomers.[5] Figure 1A shows a brightfield microscopy image of pNIPAMAAc5 microgels in solution, while Figure 1B shows an AFM image of these microgels in the dry state after being deposited from suspension on a functionalized glass surface. Note that the particles deposit on the surface and maintain the approximate lateral dimensions of the solvent swollen microgels due to strong microgel surface adhesion, resulting in mainly uniaxial deswelling in the z-dimension. Thus, the microgels appear as micron-sized disks with a thickness of only a few nanometers when imaged in the dry state via AFM. Figure 1C shows an SEM image of pNIPAMAAc5 microgels after freeze-drying a concentrated (packed) dispersion. Unlike cryo-EM, which permits the observation of hydrated samples “frozen” in their hydrated shapes/morphologies, freeze-drying does not preserve that structure. Instead, the observed morphologies of freeze-dried samples tend to be very preparation dependent, with freezing rate, dehydration rate, polymer concentration, and other factors contributing to the observed morphology. Regardless of these experimental complexities, it is sufficient to note that the image in Figure 1C shows no clear evidence of “particle-like” features and instead looks like a fibrous polymer mesh, presumably because the microgels themselves have such low intrinsic crosslinking densities and are able to interpenetrate and entangle when dried from a high concentration dispersion. In other words, the slow removal of solvent during lyophilization apparently allows for strong particle-particle interactions to evolve, giving rise to a highly interconnected mesh-like

structure. In contrast, more dimensionally stable pNIPAmBIS5 microgels shown in Figure 1D lose their distinct particle-like appearance upon freeze-drying, but produce a denser network structure associated with particle-particle “necking” type interactions. Together, these images serve to illustrate the unique nature of ULC particles that arise from their high degree of porosity and low degree of internal connectivity.

The packing of hard spheres and cross-linked microgels is fairly well understood, with numerous publications discussing their phase behavior, dynamics, and rheological properties.[7a–d, 7g, 7h, 10] For example, dispersions of cross-linked microgels undergo transitions from disordered fluids to colloidal crystals or disordered glasses at volume fractions that are similar to those of hard spheres in those states. In contrast to hard spheres, however, microgels can undergo volume decreases due to loss of solvent (deswelling), which allows for what is often referred to as “overpacking” of microgel dispersions.[2] Furthermore, it has been demonstrated that microgels possessing a low-density, “hairy” shell allow for packing through interpenetration.[7d]

ULC particles are unique due to their extremely high water content, large mesh size, and almost uniform mechanical composition; their packing behavior is expected to diverge strongly from that of hard sphere colloids. For example, the ULC morphology frequently leads to strong interpenetration and entanglement between microgels during processes such as freeze drying, as suggested in Figure 1C. From a practical standpoint, this phenomenon can make it difficult to fully redisperse ULC microgels in solution from a freeze-dried pellet, which makes controlled preparation of precise microgel concentrations difficult via that method. In our hands, it has been challenging to make ULC microgel solutions of known concentration from lyophilized samples due to poor and unreliable redispersion from the dried state.

To circumvent this redispersion problem and to study ULC microgel packing under more gentle sample preparation conditions, we interrogated ULC microgel dispersions prepared at fixed osmotic pressures. These samples were prepared by dialyzing microgel dispersions against PEG solutions of known concentrations, and hence osmotic pressures (Scheme 1). This method concentrates the microgels slowly, with the system being allowed to equilibrate for multiple weeks in each case.[11] This method also avoids the potential for aggregation or poor redispersion of particles that can arise when samples are prepared from dried solids in experiments where volume fraction is controlled gravimetrically. As compared to other methods of tuning the microgel volume fraction, external osmotic pressure variation allows us to control the concentration of ULC particles reproducibly and reliably. In our studies, the osmotic pressure was varied from 0.13 kPa to 38 kPa by dissolving different amounts of 20 kDa PEG in DI water.[12] Figure 2 shows the concentrated microgel samples following collection from the dialysis tube into glass vials. Dispersion iridescence can be observed in all cases, suggesting ordered colloidal crystal packing across the entire range of osmotic pressures.

Brightfield microscopy images of the microgel assemblies are shown in Figure 3. These images reveal the crystalline assembly of pNIPAmAAc5 ULC particles over the entire osmotic pressure range examined. As suggested by the data in Figure 1, ULC microgels

are highly swollen, loosely crosslinked networks, making them compressible via particle deswelling. Figure 3 illustrates that this deswelling and “overpacking” can be induced by simple osmotic equilibration.

To quantify the impact of osmotic equilibration on overpacking, the normalized interparticle spacing was plotted against osmotic pressure (Figure 4). Normalized interparticle spacings were calculated from the interparticle spacing at each osmotic pressure (as determined by FFT image analysis), normalized to the hydrodynamic diameter (1.1 μm) in the fully swollen state in dilute solution (as determined by DLS). We find that the ULC microgels do not deswell noticeably with increasing osmotic pressure up to ~10 kPa as shown in Figure 4A. Beyond that pressure, a sharp decrease in particle volume is observed. The elasticity of the microgel particles is an essential variable in determining microgel packing because it determines the particles’ ability to shrink in response to external stress. We can estimate the microgel stiffness from the bulk modulus or inverse compressibility utilizing the equation $K = -V \times$ slope of the osmotic pressure vs. volume of the ULC particles plot in the region where microgel starts deswelling (Figure 4B).[13] Here, V is the volume of the particles. We obtain a bulk modulus of ~11.4 kPa, which is very close to the PEG solution osmotic pressure where we first observe the deswelling of the ULC microgels (~10 kPa). This strongly suggests that particle compression during packing is connected to/controlled by the bulk modulus of the particles. This observation is supported by recent computational models of how soft particles with uniform or Gaussian crosslinking densities prefer to deform and mildly shrink with limited particle-particle interpenetration at lower generalized volume fraction.[14] Additionally, ULC particles maintain a crystalline packing arrangement even under strongly overpacked conditions, without any indication of jamming into a glassy state.[2] It has previously been reported that ultra-soft particles show a polymer-like transition in a concentrated environment.[8a] Clearly, we do not observe such behavior here, as the ULC particles continue to pack like soft colloids over the entire range of experimental osmotic pressures.

Figure 5 again shows images of pNIPAMAAc5 microgel under different osmotic pressures. The boxes on the images indicate the location of square lattices that are in coexistence with hcp colloidal crystals. It is likely that the observed square lattices are 2D planes of 3D cubic crystals, although full 3D reconstructions from DIC microscopy are not possible due to the depth of focus being a significant percentage of the particle dimension. Comparing the osmotic pressures over which we observe square lattices with the data in Figure 4A, we see that the square lattices are only present over the osmotic pressure range where the particles are uncompressed. Thus, the square lattices appear to arise only under conditions where the particle-particle interactions are dominated by the shear modulus. Particle deformation from a spherical shape can be better explained by the shear modulus (G’), which can be estimated from the crosslinking density of the ULC particles times kT, where k is Boltzmann constant, and T is the temperature. The ULC crosslinking density is estimated to be less than 0.1% which gives the shear modulus of the ULC particles, G’, significantly lower than the bulk modulus ($G' << K$). Thus, the ULC particles are expected to deform from a spherical geometry at osmotic pressures far lower than the bulk modulus. Additionally, square lattices are not observed following further compression of the crystals, where particle collapse appears to be controlled by the bulk modulus of the particles. It is important to note here

that while computational studies have previously predicted shape deformation of microgels above space filling due to interpenetration,[14] these calculations were not able to predict the specific geometric shape the particles will adopt during particle-particle interpenetration or mild shrinking.

Previous studies have suggested that charged microgels can undergo deswelling due to the osmotic pressure exerted by free counterions that migrate to the volume outside the microgels within the assembly.[7f] Given the composition of the ULC microgels used here, it is likely that ionic osmotic pressure again plays a role in the deswelling of microgels under overpacked conditions. Upon closer inspection of the images, it appears that the individual microgels adopt a cubic shape when assembled into square lattices (Figure 6), with those microgels returning to an apparently spherical shape when moving into a defect or grain boundary (a movie showing the dynamics and evolution of cubic particles in square lattices is available in the Supporting Information as Figure M1). These results suggest a delicate balance between isotropic swelling (spherical particles) and non-spherical faceting (cubic particles) to maintain crystalline packing. Again, the ULC shear modulus is significantly smaller than the bulk modulus, providing an avenue for the particles to adopt a deformed, or non-spherical shape in order to maximize the packing entropy under low osmotic pressure conditions, with particle deswelling dominating the packing behavior at pressures larger than the particle bulk modulus. Presumably, spherical particle shapes and hcp packing are driven by the maximization of entropy at the colloidal scale (hexagonal packing) and the ionic scale (particle shrinkage), whereas the cubic particles appear to optimize for a maximum volume in each particle driven by the entropy of the particles themselves. The precise mechanisms associated with the appearance of square lattices, and their stability compared with the hcp structures are currently under further investigation.

When we compare the packing behavior of ULC microgels with traditional hard sphere particles, it is clear that there are differences in their packing behavior. The packing of hard spheres is straightforward; their transition from fluid, to fluid-crystal coexistence, to closed packed structures with increasing colloid volume fractions is well established.[7g, 10, 15] On the other hand, some recent publications have suggested deformation-induced faceting of crosslinked pNIPAm microgels where the deformation was explained by the work function related to contact mechanics at low osmotic pressure.[7a, 7d] It was also proposed that crosslinked particles achieve entropic gain by minimizing their volume because of the presence of dense compact core with a very low modulus corona;[7j, 16] in this case, bcc lattices are expected to be the maximum entropy state for a certain range of volume fractions. For ULC particles, we also observe particle overpacking at particle concentrations well above random close packing for ULC, but the emergence of square lattices at lower concentrations suggests that volume maximization is important in these particles, indicating that G’ is much smaller for ULC than it is for crosslinked microgels. Taken together, our observations from ULC assemblies in packed and confined geometries deviate strongly from observations made in similar studies of crosslinked microgels or hard spheres; there are notable differences in the way ULC microgels deform, and deswell to accommodate the external osmotic pressures. While there are reports of deformation of traditional crosslinked microgels, this deformation is mainly through facet formation between adjacent microgels in their contact area under high osmotic pressure.[14, 17] In our case, the deformation of ULC

microgels not only includes the formation of cubic lattices from cubic shaped microgels in coexistence with the hcp crystals composed of spherical particles, but also reveals the spontaneous shape shifting of individual microgels from cubic to spherical shapes along grain boundaries. Thus, the existing experimental observations and theoretical predictions which can accommodate the behavior of hard spheres and crosslinked microgels fail to explain the unique behavior of ULC microgels.[7a, 7d, 14, 17–18] Qualitatively, the main differentiating factor is the extreme softness of ULC microgels relative to other systems that have been reported. In a recent publication, it was suggested that ULC microgels behave more like polymer chains in a crowded state because of their extreme softness and uniform density throughout the microgel.[19] In another report, it was claimed that the ULC microgels exhibited transient co-existence of fcc and bcc lattices at intermediate generalized volume fraction due to maximize the excluded volume and minimize the contact area between the particles.[8c] In our studies, we observe the co-existence of fcc with square lattices and a spontaneous ULC microgel shape change at grain boundaries, which might be related to an interplay between the results just referred to above and the extremely low shear modulus of the particles. We observe, however, that contact area maximization occurs in our case in a concentrated state. Our results thus call for the need for deeper investigations into the packing of ultra-soft colloidal particles, where the low shear modulus of the particles, which is orders of magnitude smaller than that controlling volume changes, is taken into account.

## 3. Conclusions

In summary, we report the synthesis and colloidal crystal assembly of ULC microgels over a wide range of packing densities. These assemblies show the co-existence of the random hexagonal close packed and cubic lattice structures at low osmotic pressure where the particles do not deswell significantly, with the samples transitioning to pure hexagonal packings as the microgels collapse under higher osmotic pressures. The appearance of the cubic lattice may relate to a balance between the low shear stiffness and the desire to maximize contact area, and the external osmotic pressure associated with free counterions favoring microgel shrinking. The dynamics of this process can be seen as ULC microgels transition from cubic to spherical shapes during their diffusion out of a cubic lattice and into a grain boundary, suggesting far greater complexity in the physics of ultra-soft sphere packing than previously observed or predicted.

## 4. Experimental Section

### Materials:

All reagents were purchased from Sigma-Aldrich unless noted otherwise. *N*-isopropylacrylamide (NIPAm) was recrystallized from hexanes and vacuum dried prior to use. Acrylic acid (AAc), ammonium persulfate (APS), potassium persulfate (KPS), and poly (ethylene glycol) (PEG, Average $M_n$=20,000) were all used as received. Deionized water (DI) was obtained from a Thermo Scientific GenPure UV ×CAD system (GmbH, Germany) and was filtered to have a minimum resistivity of 18.2 MΩ·cm. Dialysis tubes (Biotech

CE, 1000 kDa MWCO, 31 mm flat-width and BIOTECH CE, 8–10 kDa MWCO, 16 mm flat-width) were purchased from VWR.

### Poly N-isopropylacrylamide-co-acrylic acid (pNIPAm-co-AAc) ULC and Crosslinked microgel synthesis:

Microgel particles containing acrylic acid as a co-monomer were prepared with 95:5 and 90:10 ratio of co-monomers (NIPAm:AAc) (pNIPAmAAc5 and pNIPAmAAc10, respectively) with a total monomer concentration of 146 mM. N-isopropylacrylamide (NIPAm), and AAc were added to 85 mL of $H_2O$ and stirred with a magnetic stir bar. Then the solution was filtered through a 0.2 μm syringe filter into a three-neck round bottom flask. An additional 10 mL $H_2O$ was used to transfer and wash the beaker and filtered to the reaction vessel. A long waterless air condenser (CondenSyn Waterless condenser by Asynt) was placed in the center neck of the flask, and the solution was purged with $N_2$ for 1 h while the temperature was equilibrated to 70 °C with constant stirring at 480 rpm. The reaction was initiated with an APS solution (1 mM final concentration in the reaction vessel). The solution turned milky in less than 1 min, and the reaction was allowed to proceed at 70 °C for 6 h. The reaction was stopped and cooled to room temperature before filtering the solution through glass wool to remove any coagulum.

Crosslinked microgels with 90:5 ratio of NIPAm and BIS were also synthesized (pNIPAmBIS5) using protocol published elsewhere.[20] These crosslinked microgels were synthesized without the addition of any AAc.

### Purification of Microgel Particles:

Filtered microgel particles were purified via dialysis (Biotech CE Dialysis Tubing, 1000 kDa MWCO, 31 mm flat-width from VWR) against DI $H_2O$. The water was changed every day until the conductivity of the dialysate matched the conductivity of the DI water.

### Particle Characterization:

Dynamic light scattering (DLS) (Möbius, Wyatt technology) was used to determine the hydrodynamic radius ($R_H$) of the microgel particles in DI water with a small amount of added salt (5 mM $KNO_3$). The scattering data were collected for 20 s per acquisition with a total of 20 acquisitions. The data were analyzed by the Dynamics 7 software provided by Wyatt technology, where the correlation decays were analyzed using the cumulants method to calculate the diffusion coefficient, and hydrodynamic radius was determined using the Stokes-Einstein equation.

The morphology of the microgels was characterized using a Zeiss Axio Imager 2 microscope. Dilute microgel solutions were imaged by placing a drop of solution onto a microscope slide, which was then covered with a coverslip (thickness of coverslip is 1.5 mm) before placing a drop of immersion oil (refractive index 1.515) atop the coverslip. Concentrated microgel samples were loaded into rectangular capillaries (0.1 mm × 2.0 mm × 0.1 mm) known as Vitrotubes (VitroCom, NJ). Sample loading was accomplished by hand warming the microgel vessel above the microgel volume phase transition temperature (~34 °C), and then drawing the solution into the Vitrotube by capillary action. After filling

the capillary, both ends of the Vitrotube were sealed with Parafilm. The concentrated dispersion was annealed inside the sealed Vitrotube by repeatedly warming and cooling the sample across the microgel volume phase transition temperature. Vitrotube samples were examined by fixing the Vitrotube on a microscope slide with a small piece of tape. A drop of immersion oil was placed onto the Vitrotube, and the microscopic images were taken. All the images were captured using plan Apochromat 100x/1.4 oil objective in differential interference contrast mode. Micrographs were recorded and processed with imaging software ZEN (ZEN 2.5 blue edition) provided by Zeiss.

Scanning Electron Microscopy (SEM) images were taken on a Sigma 300 Electron microscope by Zeiss (Carl Zeiss Microscopy, LLC White Plains, NY). Lyophilized microgel samples were placed onto double sided tape adhered to the SEM stub and then coated with a thin layer of gold/palladium (Au/Pd 80/20%,99.99% Au/Pd) using a sputter coater model SC7620 by Quorum. Argon gas was used in the vacuum chamber (Zero Grade: 99.999%) fitted with a two-stage regulator with pressure around 5–10 psi (0.5 bar). The sputter coater was run for 45 s at 18 mA to achieve a thickness of ≈3–4 nm. Depositing a conductive thin film inhibits sample “charging”, reduces thermal damage, and enhances secondary electron emission for better imaging. The SEM operating voltage was maintained within 5–10 kV, and the SE2 detector was used with a working distance of 7–20 mm. Electron images were recorded and processed with SmartSEM imaging software provided by Zeiss.

### Osmotic Concentration of Microgels:

Purified diluted microgel solution in DI water was transferred into dialysis tubing (Biotech CE Dialysis Tubing, 8–10 kDa MWCO, 16 mm flat-width from VWR), and the open sides of the tubes were sealed with rubber bands. The PEG was dissolved in DI water without the addition of salt or buffer by gentle shaking on a shaker table. Microgel filled dialysis tubes were placed into beakers containing PEG (20 kDa) solutions of various concentrations. The concentration of PEG was varied from 0.05 % to 6% (w/v), resulting in the osmotic pressure of the solution between 0.13 kPa to 38 kPa (Figure S1).[12, 21] The volume ratio of microgel solution to PEG solution was maintained at 1:100. The microgel filled dialysis tubes were kept in the PEG solution for at least 2 weeks. No changes in microgel packing were observed following longer periods of equilibration. After this time, the microgels were transferred and stored at microcentrifuge tubes or glass vials.

### Data Analysis:

The normalized interparticle spacing was calculated using the diameter of microgels at each osmotic pressure, normalized to the hydrodynamic diameter in the fully swollen state in dilute solution. Microgels diameter at different osmotic pressures was calculated from the brightfield microscope images. Images were processed in ImageJ software (FIJI), and FFT analysis was done to calculate the particle diameter. An average of 20 particles was included in the FFT ROI to calculate the interparticle spacing.

## Supplementary Material

Refer to Web version on PubMed Central for supplementary material.

## Acknowledgments

The authors acknowledge the Keck Center High-Resolution Imaging Facility for use of the brightfield microscope, SEM, and AFM. We also thank Prof. Alberto Fernandez-Nieves (Georgia Tech, Physics) for helpful discussions. Financial support from the National Institute of Health (R01HL130918) is gratefully acknowledged.

## Data Availability Statement

The data that support the findings of this study are available from the corresponding author, [LAL], upon reasonable request.

## References

[1] a). Hoare T, Pelton R, Macromolecules 2004, 37, 2544–2550;b)Hoare T, Pelton R, Langmuir 2004, 20, 2123–2133; [PubMed: 15835661] c)Lally S, Mackenzie P, LeMaitre CL, Freemont TJ, Saunders BR, J. Colloid Interface Sci. 2007, 316, 367–375; [PubMed: 17765913] d)Wu C, Zhou SQ, Auyeung SCF, Jiang SH, Angew Makromol Chem 1996, 240, 123–136;e)Pelton R, Adv. Colloid Interface Sci. 2000, 85, 1–33; [PubMed: 10696447] f)Zhou S, Chu B, J. Phys. Chem. B 1998, 102, 1364–1371;g)Peppas NA, Merrill EW, J. Appl. Polym. Sci. 1977, 21, 1763–1770;h)Peppas NA, Mongia NK, Eur. J. Pharm. Biopharm. 1997, 43, 51–58.

[2]. Lyon LA, Fernandez-Nieves A, Annu. Rev. Phys. Chem. 2012, 63, 25–43. [PubMed: 22136621]

[3] a). Bachman H, Brown AC, Clarke KC, Dhada KS, Douglas A, Hansen CE, Herman E, Hyatt JS, Kodlekere P, Meng Z, Saxena S, Spears MW Jr, Welsch N, Lyon LA, Soft Matter 2015, 11, 2018–2028; [PubMed: 25648590] b)Douglas AM, Fragkopoulos AA, Gaines MK, Lyon LA, Fernandez-Nieves A, Barker TH, Proc. Natl. Acad. Sci. U. S. A. 2017, 114, 885–890; [PubMed: 28100492] c)Welsch N, Lyon LA, PLoS One 2017, 12, e0181369/0181361–e0181369/0181323. [PubMed: 28719648]

[4] a). Brown AC, Stabenfeldt SE, Ahn B, Hannan RT, Dhada KS, Herman ES, Stefanelli V, Guzzetta N, Alexeev A, Lam WA, Lyon LA, Barker TH, Nat. Mater. 2014, 13, 1108–1114; [PubMed: 25194701] b)Nandi S, Sommerville L, Nellenbach K, Mihalko E, Erb M, Freytes DO, Hoffman M, Monroe D, Brown AC, Journal of Colloid and Interface Science 2020, 577, 406–418; [PubMed: 32502667] c)Nandi S, Sproul EP, Nellenbach K, Erb M, Gaffney L, Freytes DO, Brown AC, Biomaterials Science 2019, 7, 669–682; [PubMed: 30608063] d)Joshi A, Nandi S, Chester D, Brown AC, Muller M, Langmuir 2018, 34, 1457–1465. [PubMed: 29257896]

[5]. Islam MR, Tumbarello M, Lyon LA, Colloid and Polymer Science 2019, 297, 667–676. [PubMed: 34103784]

[6]. Hansen CE, Myers DR, Baldwin WH, Sakurai Y, Meeks SL, Lyon LA, Lam WA, ACS Nano 2017, 11, 5579–5589. [PubMed: 28541681]

[7] a). Conley GM, Aebischer P, Nöjd S, Schurtenberger P, Scheffold F, Science Advances 2017, 3, e1700969; [PubMed: 29062888] b)Gasser U, Lietor-Santos JJ, Scotti A, Bunk O, Menzel A, Fernandez-Nieves A, Physical Review E 2013, 88, 052308;c)Hunter GL, Weeks ER, Reports on Progress in Physics 2012, 75, 066501; [PubMed: 22790649] d)Mohanty PS, Nöjd S, van Gruijthuijsen K, Crassous JJ, Obiols-Rabasa M, Schweins R, Stradner A, Schurtenberger P, Scientific Reports 2017, 7, 1487; [PubMed: 28469168] e)Paloli D, Mohanty PS, Crassous JJ, Zaccarelli E, Schurtenberger P, Soft Matter 2013, 9, 3000–3004;f)Pelaez-Fernandez M, Souslov A, Lyon LA, Goldbart PM, Fernandez-Nieves A, Physical Review Letters 2015, 114, 098303; [PubMed: 25793859] g)Pusey PN, van Megen W, Bartlett P, Ackerson BJ, Rarity JG, Underwood SM, Physical Review Letters 1989, 63, 2753–2756; [PubMed: 10040981] h)Scotti A, Gasser U, Herman ES, Han J, Menzel A, Lyon LA, Fernandez-Nieves A, Physical Review E 2017, 96, 032609; [PubMed: 29346879] i)Scotti A, Gasser U, Herman ES, Pelaez-Fernandez M, Han J, Menzel A, Lyon LA, Fernández-Nieves A, Proceedings of the National Academy of Sciences 2016, 113, 5576;j)Ziherl P, Kamien RD, The Journal of Physical Chemistry B 2001, 105, 10147–10158.

[8] a). Scotti A, Bochenek S, Brugnoni M, Fernandez-Rodriguez MA, Schulte MF, Houston JE, Gelissen APH, Potemkin II, Isa L, Richtering W, Nature Communications 2019, 10,

1418;b)Scotti A, Denton AR, Brugnoni M, Houston JE, Schweins R, Potemkin II, Richtering W, Macromolecules 2019, 52, 3995–4007;c)Scotti A, Houston JE, Brugnoni M, Schmidt MM, Schulte MF, Bochenek S, Schweins R, Feoktystov A, Radulescu A, Richtering W, Physical Review E 2020, 102, 052602. [PubMed: 33327194]

[9] a). Holden DA, Hendrickson G, Lyon LA, White HS, The Journal of Physical Chemistry C 2011, 115, 2999–3004;b)Holden DA, Hendrickson GR, Lan W-J, Lyon LA, White HS, Soft Matter 2011, 7, 8035–8040.

[10]. Hynninen A-P, Dijkstra M, Physical Review E 2003, 68, 021407.

[11]. Scotti A, Pelaez-Fernandez M, Gasser U, Fernandez-Nieves A, Physical Review E 2021, 103, 012609. [PubMed: 33601513]

[12]. Hansen PL, Cohen JA, Podgornik R, Parsegian VA, Biophys J 2003, 84, 350–355. [PubMed: 12524288]

[13] a). Liétor-Santos JJ, Sierra-Martín B, Fernández-Nieves A, Physical Review E 2011, 84, 060402;b)Sierra-Martin B, Frederick JA, Laporte Y, Markou G, Lietor-Santos JJ, Fernandez-Nieves A, Colloid and Polymer Science 2011, 289, 721–728;c)Obukhov SP, Rubinstein M, Colby RH, Macromolecules 1994, 27, 3191–3198.

[14]. Nikolov SV, Fernandez-Nieves A, Alexeev A, Proceedings of the National Academy of Sciences 2020, 117, 27096.

[15] a). Bolhuis P, Frenkel D, The Journal of Chemical Physics 1997, 106, 666–687;b)Pronk S, Frenkel D, The Journal of Chemical Physics 1999, 110, 4589–4592.

[16]. Ziherl P, Kamien RD, Physical Review Letters 2000, 85, 3528–3531. [PubMed: 11030938]

[17]. Bouhid de Aguiar I, van de Laar T, Meireles M, Bouchoux A, Sprakel J, Schroën K, Scientific Reports 2017, 7, 10223. [PubMed: 28860537]

[18] a). Gnan N, Zaccarelli E, Nature Physics 2019, 15, 683–688;b)Bergman MJ, Gnan N, Obiols-Rabasa M, Meijer J-M, Rovigatti L, Zaccarelli E, Schurtenberger P, Nature Communications 2018, 9, 5039;c)Vogel N, Retsch M, Fustin C-A, del Campo A, Jonas U, Chemical Reviews 2015, 115, 6265–6311; [PubMed: 26098223] d)Rey M, Law AD, Buzza DMA, Vogel N, Journal of the American Chemical Society 2017, 139, 17464–17473. [PubMed: 29136378]

[19]. Scotti A, Brugnoni M, Lopez CG, Bochenek S, Crassous JJ, Richtering W, Soft Matter 2020, 16, 668–678. [PubMed: 31815271]

[20]. Nayak S, Debord SB, Lyon LA, Langmuir 2003, 19, 7374–7379.

[21]. Cohen JA, Highsmith S, Biophys J 1997, 73, 1689–1694. [PubMed: 9284335]

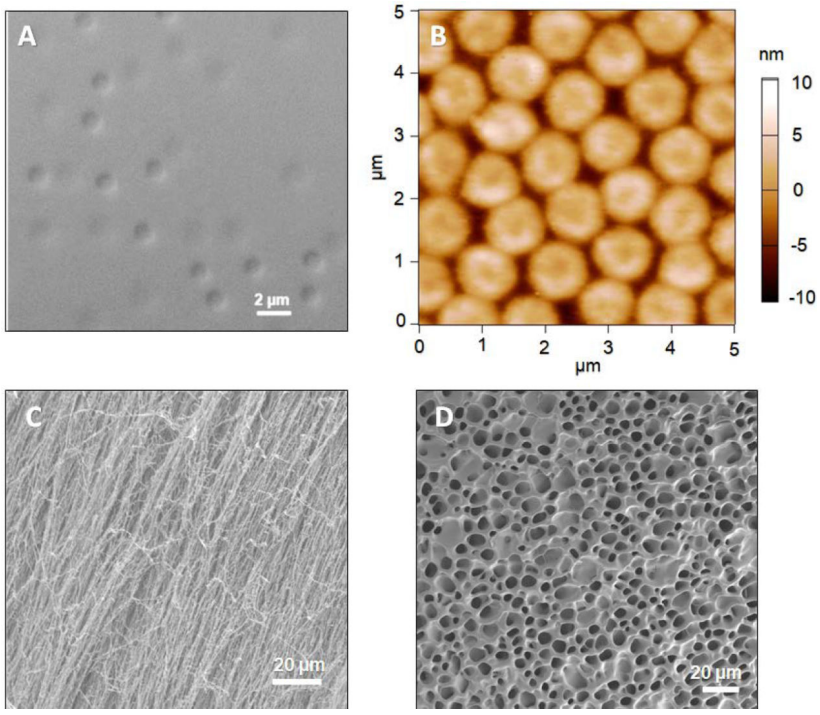


**Figure 1.**

Brightfield microscopy (A) and AFM (B) images of pNIPAmAAc5 microgels. Brightfield images were taken from a dilute microgel solution deposited on a microscope slide. A 100x/1.4 oil objective was used in differential interference contrast mode. For AFM imaging, pNIPAmAAc5 microgels were deposited on positively charged coverslips through centrifugation and AFM images were taken in their dry state. SEM images of microgels were obtained from freeze-dried, concentrated dispersions of (C) pNIPAmAAc5 and (D) pNIPAmBIS5 microgels.

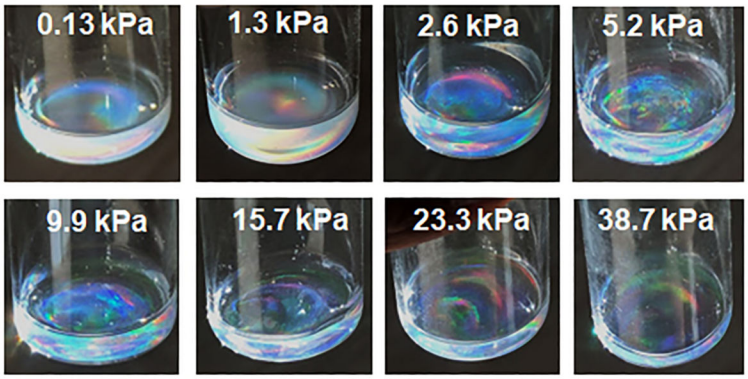


**Figure 2.**
Photographs of concentrated microgel dispersions in vials with the respective osmotic pressure used to prepare each sample indicated. The diameter of the vials is ~2.8 cm.

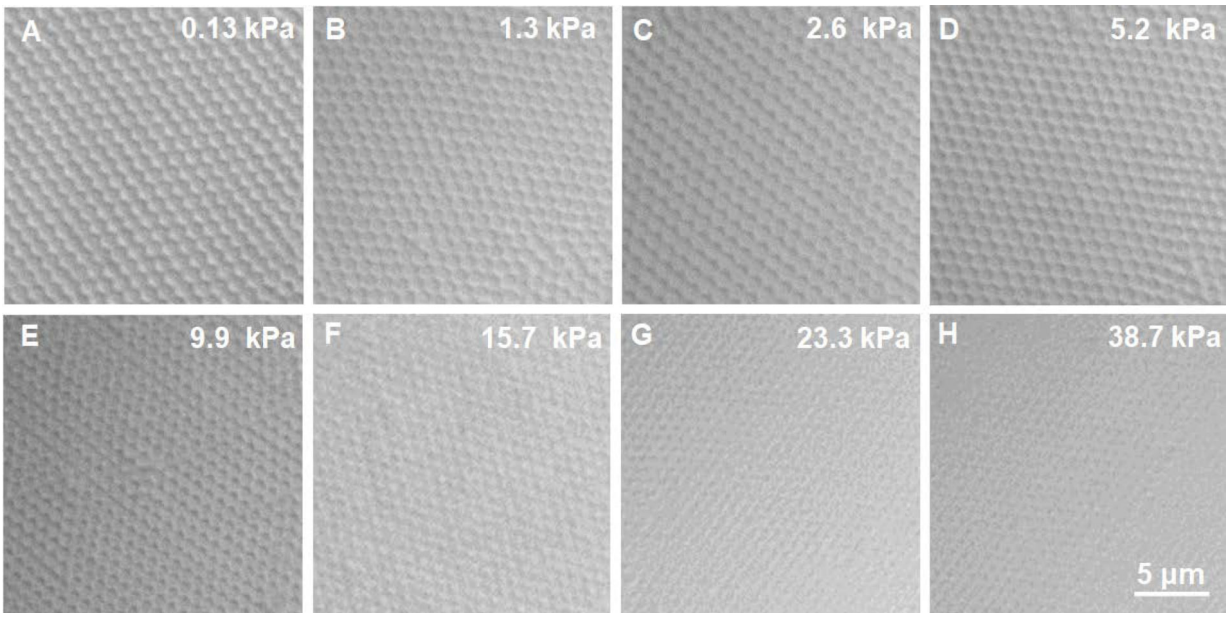


**Figure 3.**

Brightfield microscopy images of microgels concentrated under different osmotic pressures, as induced by equilibration against various concentrations of 20 kDa PEG. All images are on the same scale.

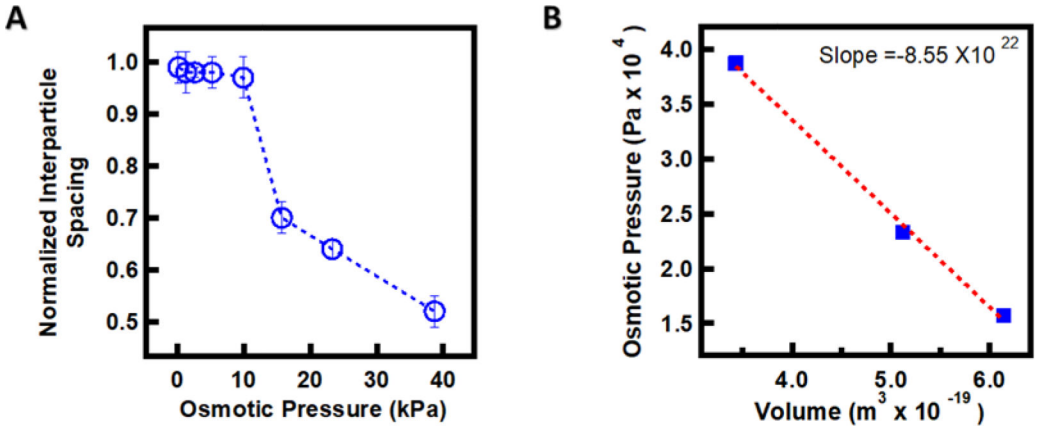


**Figure 4.**

(A) Normalized interparticle spacing vs. osmotic pressure plot of the ULCAAc5 microgels. Osmotic pressure is controlled by the external concentration of 20 kDa PEG. (B) Osmotic pressure vs. volume of the ULCAAc5 microgels in the region where the particle shrinking begins.

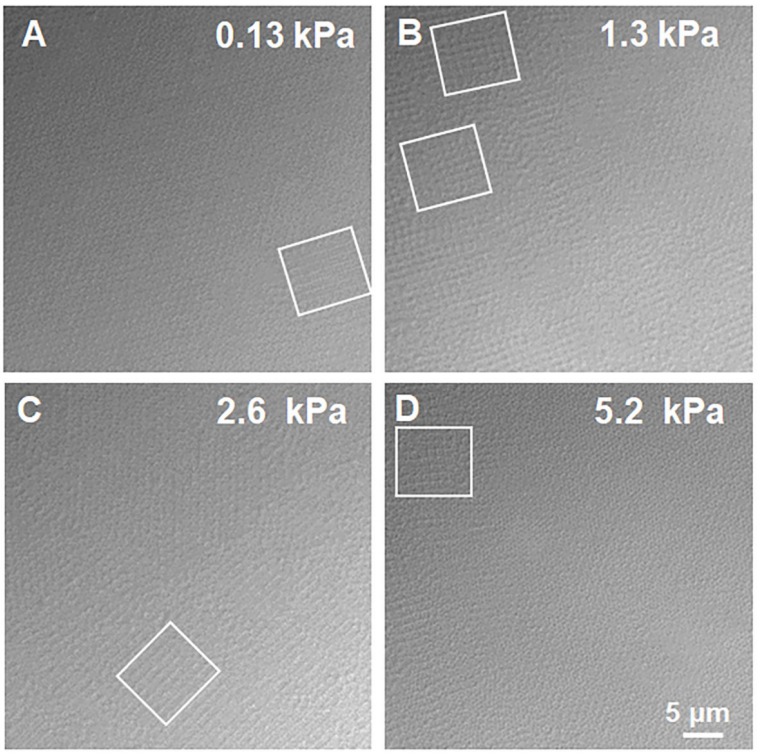


**Figure 5.**
Brightfield microscopy images of pNIPAmAAc5 microgels packing under different osmotic pressures. The images were taken by placing the microgels in Vitrotubes. The presence of the square lattices is marked with boxes. All the images are on the same scale.

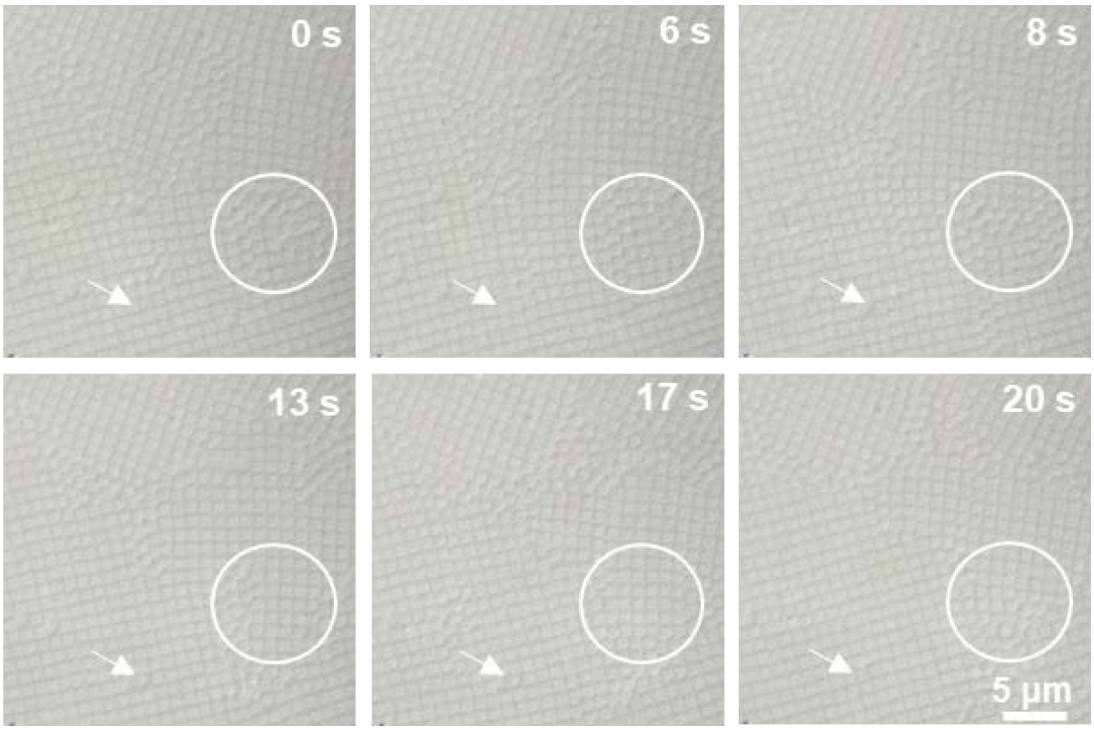


**Figure 6.**

Brightfield microscopic images of packed ULC microgels assembled into square lattices. As particles diffuse into the defects and grain boundaries, they appear to change from a cubic to a spherical shape, as indicated by the arrows. This shape change can also be clearly seen in the area marked by circle. The scale bar is same for all images.

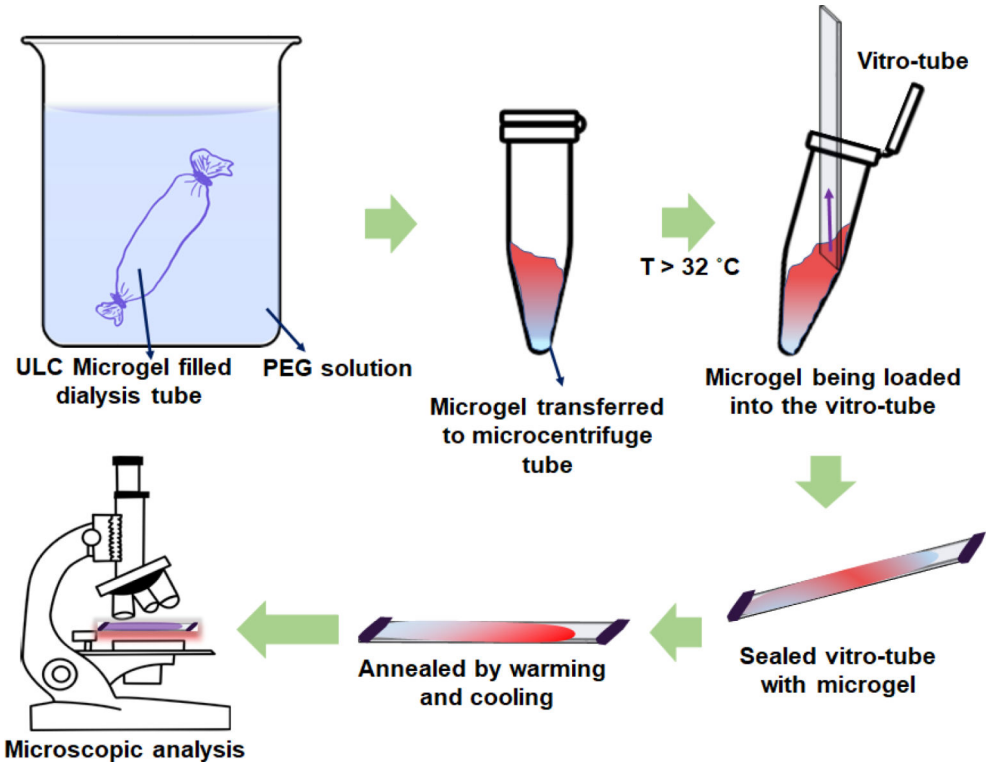


**Scheme 1.**
Sample preparation and observation